3 Molecular Crystal Project

– Precise crystal structure analysis for investigating the origin of physical properties in molecular crystals –

Project Leader: Reiji Kumai

In this project, electronic correlation in molecular crystal systems is being investigated to elucidate novel phenomena such as superconductivity and charge ordering. We will analyze the crystal structures of molecular crystals under high pressure and/or at low temperature to elucidate the origins of phase transitions.

3-1 Structural study of proton-electron-coupled organic conductors based on pyridyl-substituted tetrathiafulvalenes [1, 2]

There has been much attention on proton dynamics in hydrogen-bonded (H-bonded) molecular systems in a wide range of scientific fields from chemistry and physics to biology and materials science. For example, in an organic crystalline material, quinhydrone, proton transfer through the intermolecular H-bond associated with electron transfer between the π-electronic systems occurs, giving rise to a unique phase transition. [3] Such a proton-electron-coupled phenomenon, however, has been rarely observed in organic conductors to date. In this study, we prepared two kinds of new H-bonded organic conductor crystals **1**, **2** (Fig. 1) based on pyridyl-substituted tetrathiafulvalene (Py-TTF) molecules and discovered their proton-electron-coupled phenomenon by structural elucidation using synchrotron X-ray radiation at the beamline (BL) 8A in the Photon Factory, KEK. [1, 2]

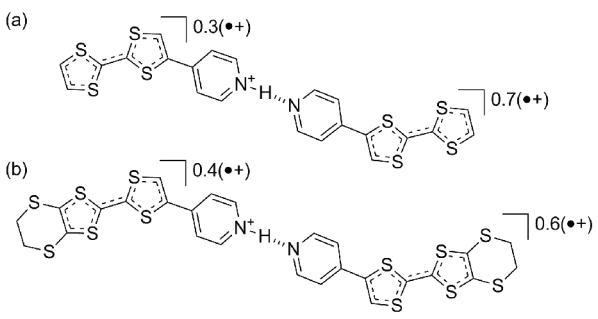

Fig. 1: Chemical structures of the H-bonded unit in (a) Py-TTF complex **1** and (b) Py-EDT-TTF complex **2**.

We first determined the crystal structure of the Py-TTF-based charge-transfer (CT) complex **1**. Interestingly, this complex has an unprecedented N^+–H···N H-bonded unit composed of two crystallographically independent Py-TTF skeletons with the N^+···N and N^+–H distances of 2.781(3) Å and 0.82(5) Å, respectively (Fig. 1a), in addition to two kinds of $F4TCNQ^{\bullet-}$ radical anion molecules and one CH_3CN as a crystal solvent. From the bond lengths of the TTF skeletons and the charge neutrality of the crystal, the valence of the TTF skeleton is estimated to be +0.3 for the PyH^+-TTF molecule and +0.7 for the Py-TTF one. Therefore, the composition of **1** is determined as (PyH^+–$TTF^{0.3+}$Py–$TTF^{0.7+}$)($F4TCNQ^{\bullet-}$)$_2$•MeCN. Furthermore, we noticed that the H-bonded proton is located close to the charge-poor (+0.3) donor within the unit structure. This is due to an asymmetric double-well potential curve for the H-bonded proton which decreases the intra-unit Coulomb repulsion between the charge-disproportionated TTF skeletons and the H-bonded proton. Owing to this proton ordering, charge-ordering occurs in the π-stacking column of the Py-TTF skeletons (Fig. 2). This result

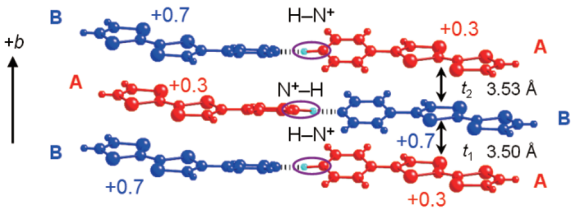

Fig. 2: The "charge-order driven proton arrangement" caused by the formation of the charge-disproportionated H-bonded unit in **1**.

demonstrates that the π-electrons in the Py-TTF donor column and the H-bonded protons between the donor columns strongly correlate each other. Thus, we called this new type of proton-electron coupled state the "charge-order driven proton arrangement". [1]

Such a unique charge-disproportionated H-bonded unit structure was also observed in the ethylenedithio (EDT)-substituted Py-TTF-based CT complex **2** (Fig. 1b) with the $N^{+}\cdots N$ and N^{+}–H distances of 2.789(4) Å and 1.18(4) Å, respectively. [2] Importantly, by this EDT substitution, the degree of the charge disproportionation is reduced from +0.3 *vs.* +0.7 in **1** to +0.4 *vs.* +0.6 in **2**, as revealed by detailed bond length analysis and DFT calculations based on the obtained X-ray diffraction data. Accordingly, the energy barrier and asymmetricity of the double-well potential curve of **2** are also lowered compared to those of **1**. These changes are clearly due to the decrease of the intra-unit Coulomb repulsion derived from expansion of the π-electronic molecular skeleton by the introduction of the EDT group, which proves the presence of a significant coupling between the π-electrons in the TTF skeletons and the H-bonded proton in the unit structure. In addition to this electronic effect, the structural effect of the EDT group, i.e. its steric bulkiness, played a crucial role in modulating the overall molecular arrangement (Fig. 3), electronic structure, and conductivity of this proton-electron-coupled organic conductor **2**. [2]

[1] S. C. Lee et al., Chem. Commun. **48** (2012) 8673.
[2] S. C. Lee et al., Chem. Eur. J. **20** (2014) 1907.
[3] (a) T. Mitani et al., Phys. Rev. Lett. **60**, (1988) 2299; (b) K. Nakasuji et al. J. Am. Chem. Soc. **113**, (1991) 1862.

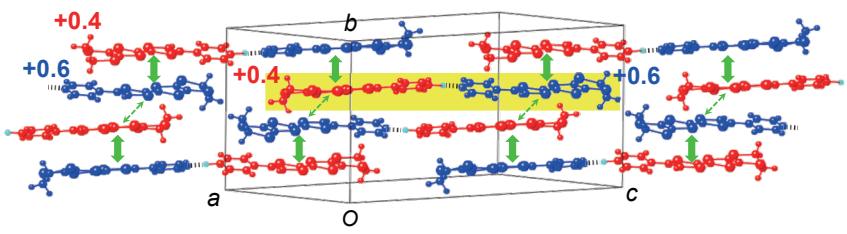

Fig. 3: Molecular arrangement of the charge-disproportionated H-bonded unit (shown in yellow) in **2**.

3-2 Structural study of SDW-CDW mixing in $(TMTSF)_2PF_6$ and charge ordering in $(TMTTF)_2Br$

In strongly correlated electron systems, the nature of insulating phases in the proximity of unconventional superconductivity is attracting attention. TMTSF- and TMTTF-based 1D organic conductors have provided a typical electronic phase diagram characteristic of the strongly correlated electron systems, the so-called Jerome phase diagram [1, 2]. In the phase diagram, charge ordering (CO), spin density wave (SDW) and superconductivity are arranged in this order as the ground states with the increase in bandwidth and dimensionality. We have performed two structural studies on the phase diagram by using the synchrotron radiation (SR) of KEK.

3-3 SDW-CDW mixing in the SDW phase of $(TMTSF)_2PF_6$

In the SDW phase of $(TMTSF)_2PF_6$, the observation of very weak satellite reflections originating from charge density wave (CDW) by employing the so-called fixed-sample-fixed-film monochromatic Laue method with a conventional X-ray source was reported [3, 4]. Since the reproducibility of the satellite observation is not so high and the *k*-space resolution of the photographic method is poor, quantitative diffraction studies using SR and a four-circle diffractometer were strongly needed.

Since TMTSF and TMTTF salts are fragile against X-ray irradiation, first we roughly estimated the modulation vector by using a hand-made rotational camera before SR experiments. Using this estimation, we limited the range of the satellite peak search and decreased the total dose of radiation applied to the sample crystals.

Figure 4 shows the satellite reflection profiles in the SDW phase ((a), (b)) and metallic phase ((c), (d)), showing the presence of CDW components in the SDW phase. The modulation vector observed is (0.5, 0.21±0.02, 0.05±0.06). The peak profile along the *c*-axis is a little broader, which may be due to weaker interaction along the axis in this material, or due to irradiation damage. The observed value of

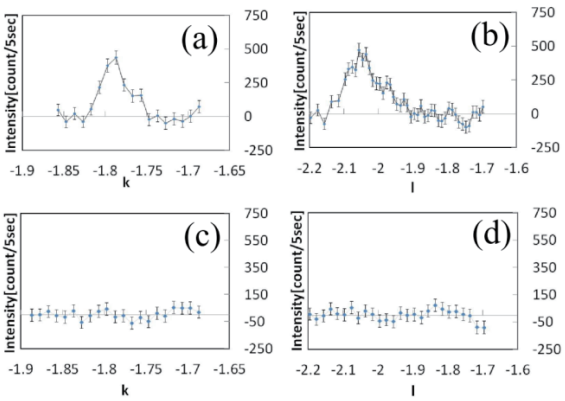

Fig. 4: Satellite reflection profiles of (0.5, 0.21, 0.05) in the SDW phase ((a), (b)) and metallic phase ((c), (d))

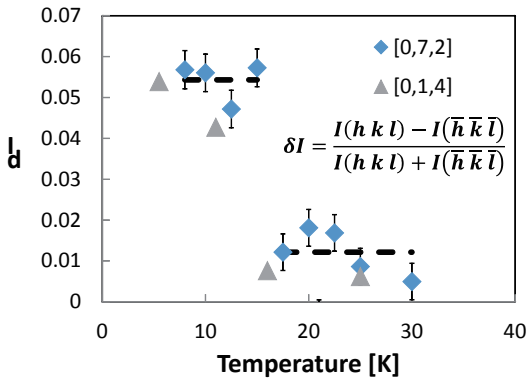

Fig. 5: Intensity difference, δI, of (0,7,2) and (0,1,4). The dashed lines are guides to the eye.

the modulation vector is consistent with that of the SDW estimated by ^{1}H-NMR [5] within experimental error.

3-4 Charge ordering in $(TMTTF)_2Br$

Although $(TMTTF)_2Br$ was considered to be placed roughly at the boundary between the CO phase and SDW phase in the unified phase diagram, the ground state had not been determined. Measurements of the spin susceptibility strongly suggested that the CO transition occurs at 20 K just above the AF transition at 14 K [6], although, due to the closeness of the temperatures, the broadening of the signal spectrum of NMR impeded a detailed study [7], and the roughness of the sample surfaces also hindered Raman analysis, which usually gives information on the degree of CO. We performed detailed crystal structure analysis of $(TMTTF)_2Br$ by using SR in order to determine the existence of CO.

Figure 5 shows the temperature dependence of the intensity difference of some Bragg reflections. Obeying Friedel's law, the intensity of the Bragg reflection of the index hkl equals that of (-h,-k,-l) for centrosymmetric crystals while a finite difference exists in non-centrosymmetric ones due to the anomalous scattering effects. The jump in the value of δI observed in Fig. 5 indicates the breaking of inversion symmetry, that is, the existence of CO, below 15 K, which is almost consistent with the AF transition temperature, 14 K.

Does this result indicate that the CO and AF transitions occur simultaneously? We don't think so, based on the results of measurements of the transport property and the spin susceptibility. The resistance of $(TMTTF)_2Br$ gradually increases below about 150 K with decreasing temperature, and rapidly increases below 20 K followed by a sharp increase below 14 K. On the other hand, the decrease in spin susceptibility starts below 20 K. The normalized resistivity between 20 K and 14 K is about 0.25–25 Ω·cm, which is quite low for that in insulating phases. This implies that the CO gap in $(TMTTF)_2Br$ is quite small and the temperature effect masks the CO, which is supported by the degree of CO, ±0.04, obtained by crystal structure analysis at 8.5 K using SR.

We performed two structural studies using SR in the phase diagram of TMTSF- and TMTTF-based organic conductors, and revealed the following two points: i) The SDW phase located between the CO and superconducting phases contains the CDW component, the modulation vector of which is almost consistent with that of SDW. ii) The ground state of $(TMTTF)_2Br$ is the CO, the degree of which is quite small.

References

[1] C. Bourbonnais and D. Jérome, Science. **281** (1988) 1155.
[2] M. Dumm et al., Phys. Rev. B. **61** (2000) 511.
[3] J. P. Pouget et al., Synth. Metals. **85** (1997)1523.
[4] S. Kagoshima et al., Solid State Commun. **110** (1999) 479.
[5] T. Takahashi et al., J. Phys. Soc. Jpn. **55** (1986) 1364.
[6] A. Ishikawa et al., Phys. Rev. B. **67** (2003) 212404.
[7] S. Hirose et al., Phys. Rev. B. **88** (2013) 125121.